Estimates of energy fluxes associated with sprites in the mesosphere

D. Mashao[1, 2, 3], M. Kosch[2, 3, 4], and M. Füllekrug[5]

[1]Department of Physics, University of KwaZulu-Natal, Durban 3629, South Africa

[2]South African National Space Agency, Hermanus 7200, South Africa

[3]Department of Physics, Lancaster University, Lancaster LA1 4YB, UK

[4]Department of Physics, University of Western Cape, Bellville 7535, South Africa

[5] Department of Electronic and Electrical Engineering, University of Bath, Bath BA2 7AY, UK

Corresponding author: Dakalo Casca Mashao (mashaodakalo@gmail.com)

Abstract

We present calibrated estimates of photon flux, lightning peak Poynting flux and Joule heating associated with the brightest region of sprites observed in the mesosphere over South Africa. The sprites' photon fluxes were estimated using 28 sprites events (observed during the 2019 sprites campaign) calibrated by stars in the sprite's image background. The lightning driven background electric field associated with the brightest region of sprites were found to vary from 0.1 to 6.7 E_k (local air breakdown field). The lightning return stroke at lower frequencies (4 Hz - 2 kHz) has more influence in carrot sprites than in column sprites formation processes. The lightning peak Poynting flux and Joule heating were estimated from calibrated electromagnetic field measurements made in parallel with eight sprites events (observed during the 2020 sprites campaign). The photon flux, peak Poynting flux, and peak Joule heating associated with the brightest region of sprites were found to be 1.1×10^{-7} W/m^2, 12.7 W/m^2, and 4.7×10^{-3} W/m^2 on average, respectively. The altitude/distance-normalised lightning peak Poynting flux decreases with increasing atmospheric altitude. The photon flux from column sprites decreased with increased altitude of the brightest region. Column sprites have a shorter time delay (<30 ms) from their parent lightning strokes than carrot sprites (up to 145 ms).

Keywords: Sprite's Joule heating, sprite's Poynting flux, sprite's photon flux, lightning return stroke.

1. Introduction

The energy from the quasi-static electric field generated mainly by large positive cloud to ground (CG) lightning discharges of Mesoscale Convective Systems (MCS) initiates collisions between electrons, neutral atoms and molecules, resulting in photon emissions forming the Transient Luminous Events (TLEs) called sprites in the middle atmosphere (Franz et al., 1990; Liu et al., 2015; Pasko, 2010; Surkov and Hayakawa, 2020). The sprites initiation process involves the downward and upward movement of streamers (Bór, 2013; Luque and Ebert, 2009). Collisions between electrons, neutral atoms and molecules lead to the emission of photons from transitions of excited states of neutral nitrogen (N_2) and ionised nitrogen (N_2^+) predominantly at an altitude above and below 50 km, respectively (Sentman et al., 1995; Heavner et al., 2010; Surkov and Hayakawa, 2012; Nnadih et al., 2021). The emissions of N_2 and N_2^+ occur as a result of excitation of the ^{1}P and 1NG states, respectively, in the ~300-1000 nm visible band (Mende et al., 1995; Hampton et al., 1996; Heavner et al., 2010). $N_2(^1P)$ has a band emission around 640 nm (~550-1070 nm wavelength range (Shibusawa and Funatsu, 2019)), with a lifetime of about 100 ms. N_2^+(1NG) has a band emission around 427.8 nm (~300-460 nm wavelength range (Heavner et al., 2010)), with a lifetime of about 5 ms (Armstrong et al., 1998; Suszcynsky et al., 1998; Heavner et al., 2010; Nnadih et al., 2021). Quenching accounts for the short lifetime of the N_2^+ emission, whereas Rayleigh scattering accounts for its low intensity (Heavner et al., 2010; Nnadih et al., 2021). The emissions of $N_2(^1P)$ and N_2^+(1NG) have lifetimes of about 6 μs and 70 ns, and quenching altitudes of about 53 km and 48 km, respectively (Heavner et al., 2010).

The altitude of the brightest region of sprites varies from 50 to 84.1 km (Füllekrug et al., 2019; Luque et al., 2016; Mashao et al., 2021; Malagón-Romero et al., 2020; Sentman et al.,1995; Stenbaek-Nielsen et al., 2010; Wescott et al., 1998; Wescott et al., 2001). The lightning electric field accelerates the electrons, and the conversion of electrons to negative ions intensifies the local electric field. The brightest region of the sprite is a region with relatively low mesospheric conductivity, enhanced electric field and electrons are converted to negative ions, which results in maximum photon production (Malagón-Romero et al., 2020; Mashao et al., 2021).

Sprites result from Joule heating of the mesosphere associated with lightning electric field (Füllekrug, 2006). Füllekrug et al. (2006) reported on stratospheric Joule heating determined

from the lightning continuing current measurement. They found that the Joule heating varied from 1×10^{-4} J/m^3 to 1×10^{-8} J/m^3 for altitudes ranging from 25 to 45 km, respectively (Füllekrug et al., 2006). Gordillo-Vázquez et al. (2018) investigated, by spectroscopic means, the temperature of mesospheric regions between 65 km and 76 km and found no measurable heating associated with sprites. We are not aware of any reported estimates in the literature of lightning Joule heating and Poynting flux in the mesosphere in relation to sprites.

For non-delayed sprites to occur the lightning driven electric field must exceed the local air breakdown field (120 Townsend (Td)) (Pasko et al. 2013; Surkov and Hayakawa, 2020). However, the lightning driven electric field lower than the local air breakdown field can lead to delayed sprites due to associative detachment (Luque and Gordillo- Vázquez, 2012).

We evaluate lightning initial apparent peak Poynting flux and Joule heating projected to the altitude of the brightest regions of sprites in the mesosphere for the first time. We also compare photon flux at the altitude of the brightest region of the optical observations column and carrot sprites using a camera with a red (N_2) emission filter. The lightning-driven electric field associated with the altitude of the brightest regions of sprites were determined and compared with the published literature.

2. Optical and radio recordings

The reported sprites were recorded during the 2019 and 2020 sprites campaigns from the Square Kilometre Array (SKA) (30.97º S, 21.98º E) and the South African Astronomical Observatory (SAAO) (32.38º S, 20.81º E), Northern Cape, South Africa. The sprites were observed on the following nights: 01 February 2019 from SKA and 24 January 2020 from SKA and SAAO. Figure 1 shows the map of South Africa, the MCS associated with some of the observed sprites, and the SKA and SAAO sites marked with red and yellow dots, respectively. The +CG, -CG, and IC lightning discharges are marked with plus, negative, and dash-like symbols within the thundercloud, respectively. Lightning electric field observations were made in 2019 and 2020. Lightning magnetic field observations were made in 2020 only. Eight sprites events with no calibrated stars present were recorded during the 2020 sprites campaign and are used for estimating the lightning Poynting flux and Joule heating associated with the altitude of the brightest regions of sprites only. The 2020 sprites campaign data comprised of column, carrot, wishbone, jellyfish, tree, angel, and sprites with halo. From the 2019 sprites campaign, we selected column and carrot sprites that occurred individually or in a group with calibrated stars of known photon flux. We found 14 column

and 14 carrot sprites red emission optical data with calibrated stars and used them for estimating the photon flux as well as Joule heating (Alekseeva et al., 1996; Bór, 2013).

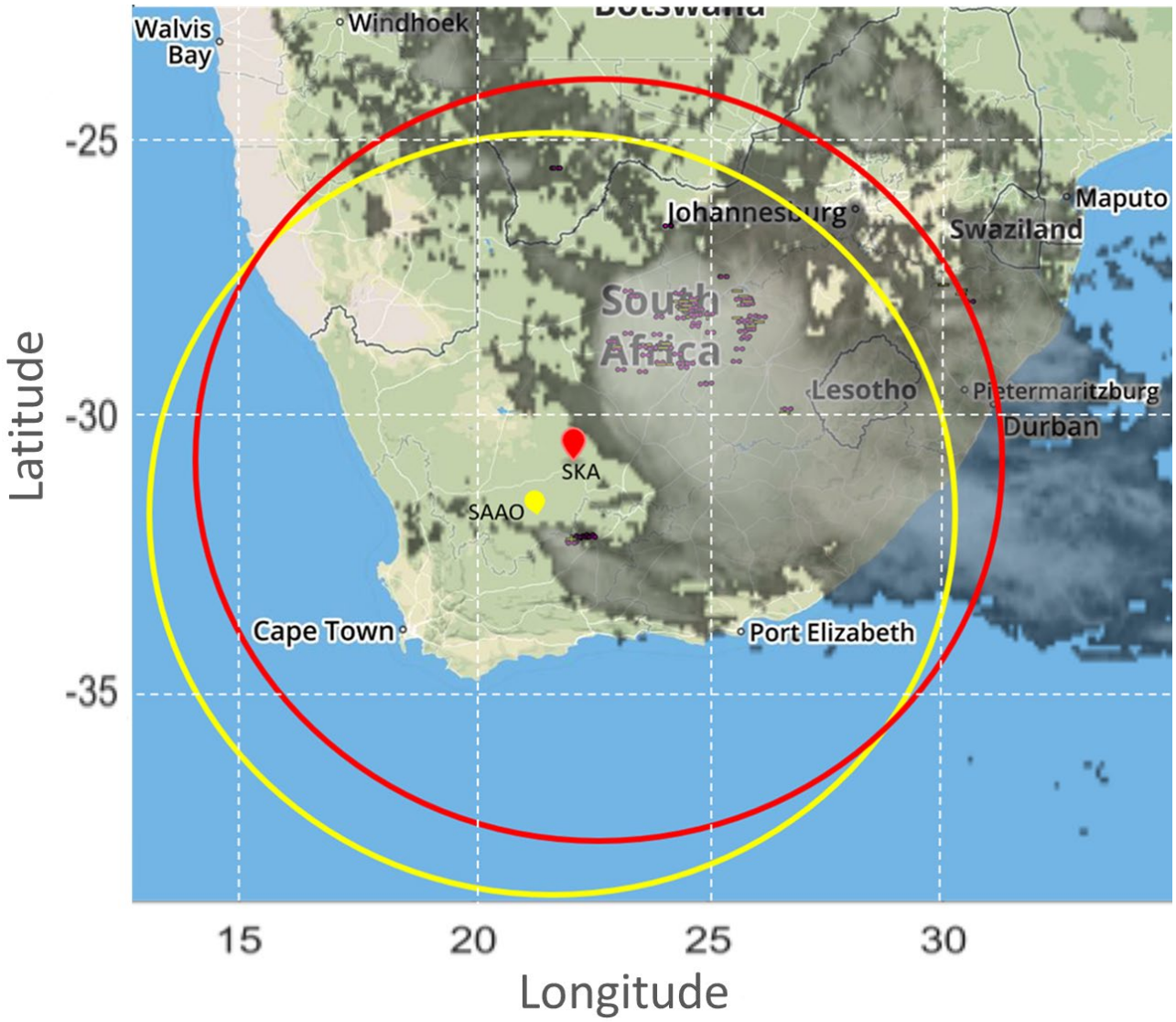

Figure 1. Map of South Africa captured on 1 February 2019 at 22:41:00 UTC. The SKA/ SAAO sites are marked with red/yellow dots, and the MCS associated with some observed sprites is shown in grey. The circles mark the 900 km radius, which is the maximum distance our cameras can observe from SKA and SAAO, respectively (Earthnetworks.com, 2020).

2.1 Optical recording

Watec 910Hx and Allied Vision Pike night vision cameras, mounted on the same tripod, were used to record the sprites from SKA/SAAO (Mashao et al., 2021; Nnadih et al., 2018, Nnadih et al., 2021). The stars in our field of view (FOV) were utilised to co-align the cameras. The cameras' viewing directions were North, East, and South of SKA and SAAO.

The Watec 910Hx cameras, with an 8.0 mm f/1.4 C-mount lens, operated with 0.45 gamma factor and 8-bit intensity resolution. The Watec 910Hx cameras recorded 25 video frames per second (fps) with a 40 ms frame period. A Global Positioning System (GPS) video timer provided time with millisecond timing to the camera system. The Watec 910Hx cameras had a 29°/46.2° FOV Vertical/Horizontal (V/H), 0.061°/0.072° V/H angular resolution per pixel, and 640×480 (H×V) pixels.

The Allied Vision Pike camera, coupled to a Ceramic xx1332 Mullard image intensifier with Xenon F0.95 50 mm C-mount TV lens, captured images at 25 fps and a 40 ms frame period, 640×480 video image size, 15°/21° FOV V/H, and 14-bit intensity resolution. The Ceramic xx1332 Mullard image intensifier has wavelength range of about 360 nm to 850 nm (Allied Vision, 2022; Worthpoint, 2022). A red N_2 longpass cut off filter with a 640-650 nm was used to record the $N_2(^1P)$ emission of sprites. A Network Timing Protocol server provided timing accuracy of about 1 ms for the Pike camera system at SKA.

2.2 Electromagnetic recording

The lightning electric (2019 and 2020 campaigns) and magnetic (2020 campaign only) fields were recorded in parallel with sprites optical recordings at SKA. A wideband digital ELF/VLF/LF radio receiver that detected the lightning vertical electric field strength observed with about 4 Hz to 400 kHz frequency range, with a sampling frequency of 1 MHz, and timing accuracy of 20 ns (Füllekrug, 2010; Füllekrug et al., 2019). The lightning magnitude values were converted to Td by using the modelled N_2 densities associated with the targeted sprites altitude. We then obtain the ratio between the lightning electric field and local air breakdown field (E_k), see Tables 1 to 4. All N_2 densities are obtained from the NRLMSISE profile (https://ccmc.gsfc.nasa.gov/modelweb/models/nrlmsise00.php). Two orthogonal induction coils are used to record the horizontal magnetic field in the frequency range of ~4 Hz to ~60 kHz with a sampling frequency of 500 kHz and a timing accuracy of ~20 ns. Lightning magnetic field observations were conducted during the 2020 sprites campaign only from SKA.

The Earth Network Total Lightning Network (ENTLN) and South African Lightning Detection Network (SALDN) provided lightning data (time, position, peak current, type of discharge, and polarity) related to the observed sprites. ENTLN and SALDN have position accuracy of about 0.2 km and 0.5 km, respectively (Gijben, 2012; Bui et al., 2015; Zhu et al.,

2017). All CG lightning events associated with the sprites reported here have positive polarities. The peak lightning current varied from 28 to 142 kA, see Tables 1 to 4.

3. Data analyses

3.1 Sprite altitude estimation

We estimate the lightning peak Joule heating and apparent Poynting flux, and average photon flux associated with the sprites brightest regions using optical data as well as lightning electric and magnetic field data. The right ascension and declination of stars on the sprites image background and the geographic position of the camera were used to determine the azimuth angle, elevation angle, and field of view of the cameras. The azimuth and elevation angles of stars were computed and used to fit onto the real stars in the background image of sprites. The altitude of the sprite's brightest region was obtained by employing spherical and planar trigonometry in the horizontal and vertical planes, respectively (Mashao et al., 2021; 2022a; 2022b), assuming that the sprites events occurred directly above their parent lightning locations. The latter assumption is commonly used in sprites optical research (Füllekrug et al., 2019; Li et al., 2008; Luque et al., 2016; Mashao et al., 2021; 2022a; 2022b; McHarg et al., 2007; Stenbaek-Nielsen and McHarg, 2008). The uncertainty in altitude of sprites computed from the angular resolution of the camera spanned from ± 0.33 to 0.47 km. The uncertainty in the altitude of sprites varies with slant distance from the location of camera to the sprites.

3.2 Poynting flux estimation

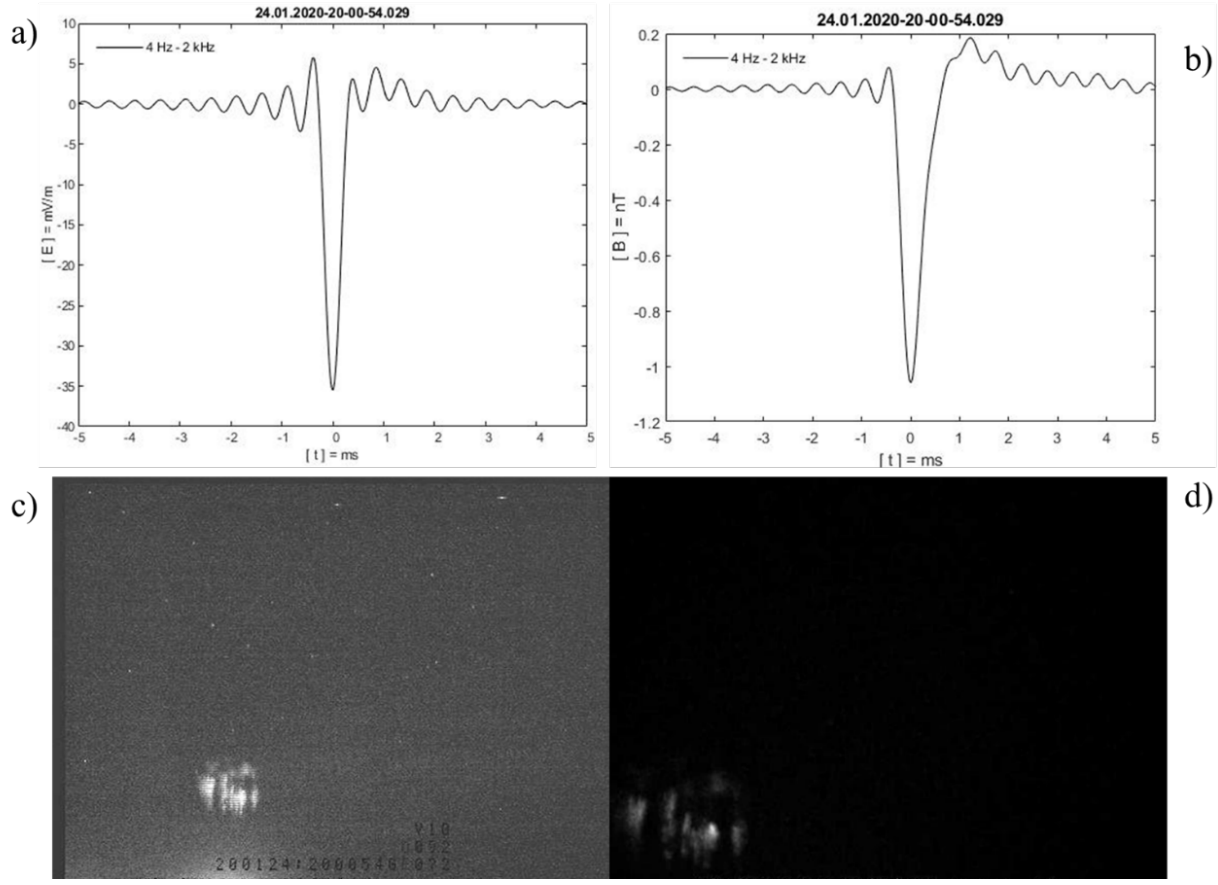

Figure 2. The lightning electric (a) and magnetic (b) waveforms associated with the sprite event observed on 24 January 2020 at 20:00:54.072 UTC from SKA recorded by monochrome camera without a filter (c) and with a red N_2 filter (d). The correct sprite event time stamp is displayed on the image with no filter.

Figure 2 shows the lightning electric (a) and magnetic (b) field waveforms associated with the sprites event recorded simultaneously by a monochrome camera without a filter (c) and with the red N_2 filter (d) from SKA. We used the simultaneous lightning peak electric and magnetic field strengths associated with the optical sprites to determine the maximum apparent Poynting flux associated with the eight sprites analysed in the frequency range of 4 Hz to 2 kHz. The Poynting flux (**S**) is given by (Farrell et al., 2006):

$$\mathbf{S} = \frac{(\mathbf{E} \times \mathbf{B})}{\mu} \quad (1)$$

where (**E**) is the lightning electric field, (**B**) is the lightning magnetic field, and (μ) is the permeability of the medium. The free space wave impedance is modified near a conductor, in this case the Earth, which is studied in the field of magnetotellurics in detail (Bór et al. 2022). Here we assume a vacuum. To compare the lightning electric and magnetic field strengths, we filter the data to obtain the lightning return stroke at lower frequencies information (4 Hz - 2 kHz), see Figure2 (a) and (b) (Constable, 2016; Cummer et al., 2013; Fraser-Smith and Bowen, 1992; Füllekrug, 2010). ELF/VLF/LF lightning radio receivers with lower minimum frequency (<4 Hz) are required to measure lightning continuing current. These data are not available to us. Lightning continuing current plays an essential role in initiating delayed sprites, sustaining the quasi-static electric field in the mesosphere and the brightness of sprites longer than the local relaxation time (Gomez Kui et al., 2021; Kitagawa et al., 1962; Ren et al., 2021; Tomicic et al., 2021).

Due to a technical problem, we only recorded the dominant horizontal component of the magnetic field aligned in the North-South geographic direction. Since the lightning occurred between 209.5 and 562.3 km away from the receiver, we used Equation (2) to estimate the total horizontal magnetic field ($\mathbf{B_T}$):

$$\mathbf{B_T} = \mathbf{B}/\sin(AZ) \quad (2)$$

where *AZ* is the azimuth angle between the lightning position and the North-South coil orientation.

The radiation field terms decrease as 1/d, $1/d^2$, and $1/d^3$, depending on the horizontal distance between the lightning event and the receiver, where d is the distance from the lightning location to the receiver location (Cooray and Lobato, 2020). At short distances, radiation field terms decrease as 1/d, and $1/d^2$.

From the recorded data, we estimate the lightning electric and magnetic fields associated with the altitude of the brightest regions of sprites. The lightning electric and magnetic fields associated with the altitude of the brightest regions of sprites were normalised as follows: We project horizontally the lightning electric and magnetic radiated fields as $1/d^2$, to 1 km away from the lightning location (Cooray and Lobato, 2020; Taylor and Jean, 1959). This was done by multiplying the observed lightning electric and total magnetic field values by the distance squared in km. For our geometry, the parent lightning source of the fields is assumed to be a finite line current. It is known that the lightning quasi-static electric field strength, which may

initiate sprites, lessens with increasing altitude as $\frac{1}{a^3}$, where a is atmospheric altitude (Pasko et al., 2013). We assumed that the CG lightning charges, which initiated the sprites events, were removed at 10 km altitude (Asano et al., 2008; Pasko et al., 2013), and we then determined lightning electric (E_s) and magnetic field strength associated with the sprite's brightest region altitude as $\left(\frac{10}{a}\right)^3$, where a is the calculated altitude (km) of the sprite's brightest region (see example in the Appendix). Finally, we obtain the distance/altitude-normalised peak apparent Poynting flux associated with the sprite's brightest region altitude using Equations 1 and 2. The lightning peak Poynting flux associated with the altitude of the brightest regions of sprites estimates are presented in Table 1 (see Appendix). An example calculation of the lightning peak Poynting flux associated with the altitude of the brightest regions of sprites is presented in the Appendix.

3.3 Joule heating estimation

To determine the lightning Joule heating associated with the sprite's brightest region altitude, we used the lightning electric field strength (**E**) and the atmospheric conductivity (**σ**) adopted from Liu et al. (2015), integrated over the observed vertical extent of the brightest region of the sprites. The vertical extent of the brightest region of sprites spanned from 1.2 to 2.4 km. Joule heating ($\mathbf{J_h}$) is given by (e.g. Kosch and Nielsen, 1995; Foster et al., 1998):

$$\mathbf{J_h} = \boldsymbol{\sigma}\mathbf{E}^2 \quad (3)$$

The same altitude/distance normalised lightning electric field data used to estimate the peak Poynting flux was used to determine the peak Joule heating (first-order approximation). The atmospheric conductivity corresponding to the vertical extent of the brightest region altitude of sprites was used to calculate the lightning peak Joule heating associated with the altitude of the brightest regions of sprites using Equation (3). Sprite streamer formation involves ionisation of the neutral atmosphere, which will modify the local conductivity and electric field within the sprites. Hence, we can only estimate the initial peak Joule heating before streamer ionisation takes over. The atmospheric conductivity was obtained from rocket measurements, which have been used in other TLE studies (Holzworth et al.,1985; Liu, 2012; Liu et al., 2015). For the 2019 sprites campaign, the height-integrated atmospheric conductivity varied from 1.2×10^{-6} to 2.1×10^{-4} S, for altitudes ranging from 61.5 to 75.3 km. For the 2020 sprites campaign, the height-integrated atmospheric conductivity corresponding to the column and carrot sprites' brightest region altitudes varied from 1.1×10^{-7} to 1.1×10^{-5} S,

for altitudes ranging from 53.1 km and 69 km. The values of conductivities used here are lower limits.

Dowden et al. (2001) used measurements of VLF scattering in millisecond time scale, through horizontal angles of up to 180° to demonstrate that the sprites plasma has high conductivity. They set an approximate lower bound for conductivity of sprites plasma to 3×10^{-7} S/cm. Liu et al. (2009b) sprite simulations were extrapolated by Luque and Ebert (2010) which showed conductivity of about 8×10^{-8} and 5×10^{-8} S/cm, respectively. The sprite conductivity increases in time with respect to the background and the re-enhancement of the electric field in the sprites' streamer wake results in further increase in conductivity (Gordillo-Vázquez and Luque, 2010).

The lightning initial peak Joule heating is due to the lightning discharge within the bandwidth of the measured electric field (4 Hz – 2 kHz), corresponding to the lightning return stroke, and atmospheric conductance, corresponding to the vertical extent of the brightest region altitude of sprites. The results of lightning peak Joule heating associated with the altitude of the brightest regions of sprites estimate are shown in Tables 2, 3, and 4 (see Appendix). An example calculation of the lightning peak Joule heating associated with the altitude of the brightest regions of sprites is presented in the Appendix.

3.4 Photon Flux

To determine the sprite's photon flux out of the brightest region, we acquired sprites optical data observed with red N_2 emission filter simultaneously with calibrated stars of known photon flux (in W/m^2), as described in detail by Nnadih et al. (2021). The flux values of selected stars can be found in the Pulkovo Spectrophotometry Bright Stars Catalogue (Alekseeva et al., 1996). Only the sprites recorded during the 2019 sprites campaign from SKA had images containing calibrated stars. Figure 3 shows an example of a recorded sprite with calibrated star.

Figure 3. Images recorded with no filter (left) and red N_2 (right) filter on 01 February 2019 at 19:08:24.202 UTC from SKA. The images contain the same sprites event. The red circle in the image on the right denotes the calibrated star. The correct sprite event time stamp is displayed on the image with no filter.

We can estimate photon flux since we recorded the sprites events and the stars simultaneously with fixed camera gain setting and similar atmospheric losses over the same night. We averaged the sprites video clip frames over one second in order to determine the average intensity pixel value of the calibrated star ($\mathrm{Str_{avg}}$). The sky background ($\mathrm{Sky_{bkg}}$) value was obtained by using a 7×7 median filter to remove the stars on the video frame prior to the frame which contained the sprites event. To determine the sprite's average brightness ($\mathrm{Sprs_{avg}}$), we average the image pixel values over the sprite's brightest region altitude range. The average intensity pixel value ($\mathrm{Str_{avg}}$) and known photon flux value of the calibrated star ($\mathrm{Str_{flux}}$, integrated over the filter's longpass), sky background ($\mathrm{Sky_{bkg}}$), and the average image intensity pixel value over the sprite's brightest region altitude range ($\mathrm{Sprs_{avg}}$) were used to obtain the photon flux at the sprite's brightest region ($\mathrm{Sprs_{flux}}$), by means of Equation (4) (Nnadih et al., 2021).

$$\mathrm{Sprs_{flux}} = \frac{\mathrm{Str_{flux}}(\mathrm{Sprs_{avg}} - \mathrm{Sky_{bkg}})}{\mathrm{Str_{avg}} - \mathrm{Sky_{bkg}}} \ (\mathrm{W/m^2}) \qquad (4)$$

An example of the photon flux calculation at the sprite's brightest region is presented in the Appendix. The estimated column and carrot sprites' photon flux are shown in Tables 3 and 4 in the Appendix.

4. Results and discussion

The radiated electric fields of lightning discharges associated with 8 sprites events for the 2020 campaign (Table 1) at the ELF/VLF/LF receiver, projected to 1 km from the lightning position at ground level, and projected to the sprites' brightest region altitude varied from 2.6×10^{-3} to 5.7×10^{-1} V/m, 454.1 to 25059.6 V/m, and 1.1 to 68.9 V/m, respectively. The radiated magnetic field of lightning discharges associated with 8 sprites events for the 2020 campaign (Table 1) at the receiver, projected to 1 km from the lightning position at ground level, and projected to the sprites' brightest region altitudes varied from 2.95×10^{-10} to 1.09×10^{-9} T, 5.26×10^{-5} to 6.33×10^{-4} T, and 1.23×10^{-7} to 2×10^{-6} T, respectively. The radiated electromagnetic fields values are associated with the lightning return stroke at lower frequencies (4 Hz - 2 kHz). The radiated lightning electric and magnetic fields uncertainties were about ±0.05 V/m and $\pm2.5\times10^{-8}$ T, respectively, at the sprites' brightest region altitudes. Uncertainties associated with the use of first-order distance projection estimates are not included. The estimated altitude of the brightest region of 8 sprites events ranged from 61.5 to 75.3 km. The altitude of the brightest region of sprites is within that previously reported (i.e. 50 - 84.1 km) (Füllekrug et al., 2019; Luque et al., 2016; Mashao et al., 2021; Malagón-Romero et al., 2020; Sentman et al.,1995; Stenbaek-Nielsen et al., 2010; Wescott et al., 1998).

The N_2 density at the altitude of the brightest region of sprites (61.5—75.3 km) varied from 6.85×10^{14} to 4.39×10^{15} cm^{-3}, see Tables 1 and 2. All N_2 densities are obtained from the NRLMSISE profile (https://ccmc.gsfc.nasa.gov/modelweb/models/nrlmsise00.php). The altitude/distance normalised lightning driven peak electric field (E_s) at the altitude of the brightest region of sprites spanned from 0.1 to 0.5 E_k, associated with the lightning electric field in the frequency range 4 Hz to 400 kHz. The frequency range 4 Hz to 400 kHz provides the lightning electric field information that the ELF/VLF/LF radio receiver can measure. These E_k values fall into the range reported the literature (Gamerota et al., 2011: Hu et al., 2007; Kanmae et al., 2012; Li and Cummer, 2012). The E_s at the altitude of the brightest region of sprites associate with the lightning return stroke at lower frequencies (4 Hz - 2 kHz) varied from 0.01 to 0.4 E_k. The reduction of the lightning driven electric field is due to filtering of the lightning electric fields data to obtain the lightning return stroke fields at lower frequencies. Gamerota et al. (2011) model demonstrated that a lightning electric field of 0.08 E_k is not sufficient to produced sprites. However, Gamerota et al. (2011) model

330 doesn't consider the intracloud lightning electric field which enhances the electric field
331 energy at sprites altitudes (Füllekrug et al., 2019). The electric field energy might make it
332 possible for lightning discharges with 0.08 E_k or less to initiate sprites. The lower E_k may be
333 due to lower temporal resolution of the observations (Pasko et al., 2013). We note that some
334 of our analysed E_s values are greater than the previous reports (Gamerota et al., 2011; Hu et
335 al., 2007; Li and Cummer, 2012). However, the E_s values are within the same order (3-5
336 times the E_k) obtained by Kanmae et al. (2012) for sprites streamers peak electric field. Our
337 peak electric field values are the background estimated electric field associated with the
338 altitude of the brightest region of sprites. During sprites formation processes, conversion of
339 electron to negative ions intensifies the electric field (Malagón-Romero et al., 2020; Mashao
340 et al., 2021). The electric field value of about 8 E_k has been associated with gigantic jet
341 discharge (Kuo et al., 2009; Pasko et al., 2013). None of our events are gigantic jets, as
342 confirmed by the cameras.
343
344 For the same 8 sprites, the lightning peak apparent Poynting flux (see Table 1) associated
345 with the sprite's brightest region, using distance/altitude normalised data, was found to span
346 from 0.6 to 30.1 W/m^2 (0.08 W/m^2), with an average of 12.7 W/m^2. The value in parentheses
347 is the uncertainty. Figure 4 shows the peak Poynting flux associated with the brightest region
348 of sprites increased with decreasing atmospheric altitude. The linear correlation coefficient
349 between these variables is -0.7. This outcome is expected as both the electric and magnetic
350 fields decrease as $\frac{1}{a^3}$ with increasing altitude.

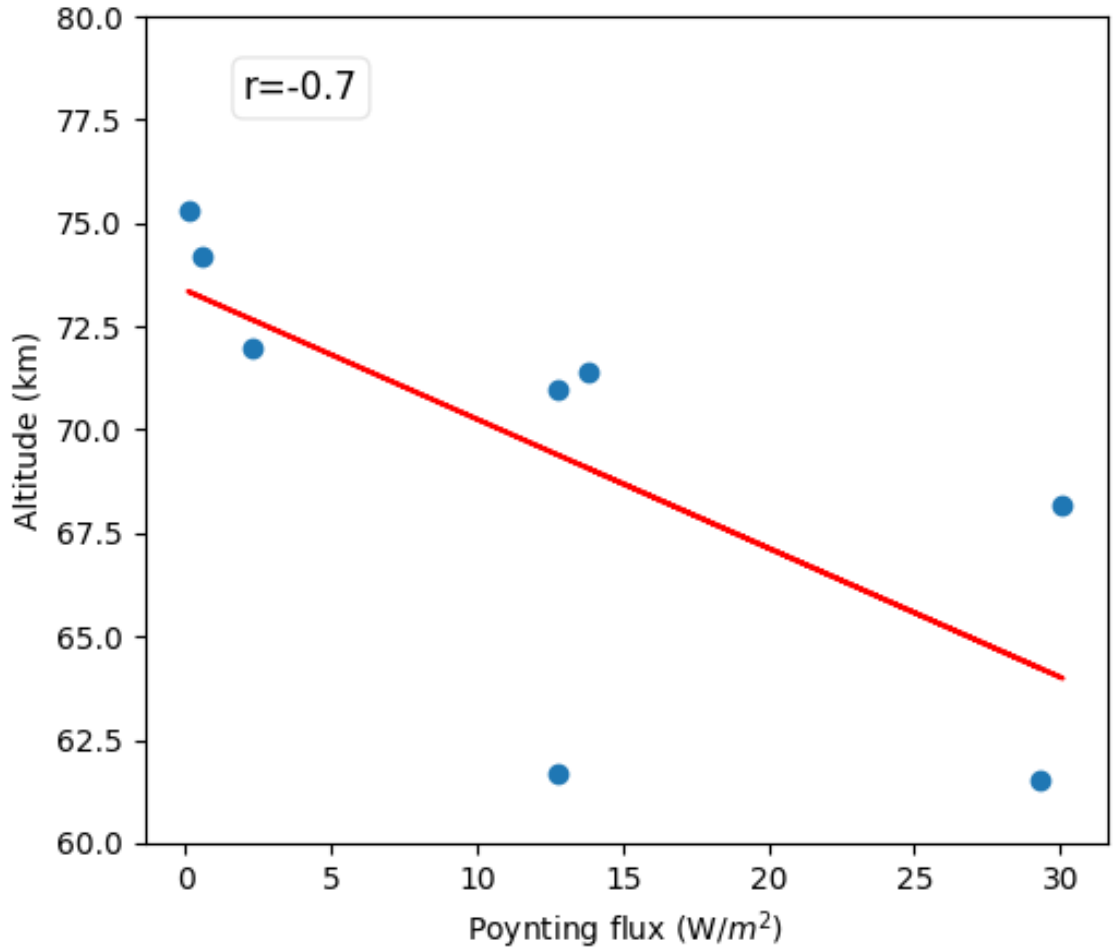

Figure 4. The relationship between the distance/altitude normalised lightning peak apparent Poynting flux associated with the brightest region of sprites and atmospheric altitude. r shows the linear correlation coefficient.

For the same 8 sprites, for the estimates of lightning initial peak Joule heating (see Table 2) associated with the sprites' brightest region, we used the atmospheric conductivity values from Liu et al. (2015), integrated over the vertical extent of the brightest region of the sprites. The vertical extent of the brightest region of sprites varied from 1.2 to 2.4 km. The altitude/distance normalised initial peak Joule heating ranged from 2.6×10^{-5} to 1.4×10^{-2} W/m^2 ($\pm2.4\times10^{-6}$ W/m^2) over the same altitude range (61.5 – 75.3 km). The value in parentheses is the uncertainty. The average peak Joule heating was found to be 4.7×10^{-3} W/m^2. The initial peak Joule heating associated with sprite's brightest region altitude decreases with an increase in atmospheric altitude, with a linear correlation coefficient of -0.4 (not shown). This outcome is expected as the electric field decreases as $\frac{1}{a^3}$ with increasing

366 altitude. A linear correlation coefficient of -0.04 was found for the E_s/E_k and altitude of
367 brightest region of sprites (not shown).
368
369 From the 2019 campaign (see Tables 3 and 4), the N_2 red photon flux from the sprites (14
370 column and 14 carrot sprites) brightest region spanned from 2.5×10^{-8} to 2.7×10^{-7} W/m^2
371 ($\pm2.5\times10^{-9}$ W/m^2) with an average value of about 1.1×10^{-7} W/m^2, for altitudes between 53 to
372 69 km. The value in parentheses is the uncertainty. There is no significant linear correlation
373 between the peak photon flux of sprites and atmospheric altitude, with a correlation
374 coefficient of -0.2 (not shown).
375
376 The apparent radiated lightning peak electric field at the column and carrot sprites' brightest
377 region altitudes ranged from 59.9 to 479.6 V/m and 22.3 to 438 V/m, respectively, for
378 altitudes between 53.1 and 69 km. The average apparent radiated lightning electric field
379 within the column and carrot sprites were 193.3 and 190.4 V/m, respectively. The sprites
380 associated with radiated lightning electric field lower than the breakdown electric field (120
381 Td) may be generated due to associative detachment (Luque and Gordillo- Vázquez, 2012).
382 The radiated electric field values are associated with the lightning return stroke at lower
383 frequencies (4 Hz - 2 kHz). For the lightning electric fields in the frequency range 4 Hz to
384 400 kHz, the apparent radiated lightning peak electric field at the column and carrot sprites'
385 brightest region altitudes varied from 537.4 to 2727.9 V/m and 596.9 to 2477.9 V/m,
386 respectively, for altitudes between 53.1 and 69 km. These values are consistent with the
387 expected quasi-electrostatic field produced by lightning in the mesosphere (Liu et al., 2009a).
388
389 The N_2 number density at the altitude of the brightest region of column and carrot sprites
390 (53.1—69 km) vary from 1.67×10^{15} to 1.27×10^{16} cm^{-3}. For column sprites, the E_s at the
391 altitude of the brightest region ranged from 0.6 to 5.8 E_k (4 Hz to 400 kHz) and 0.1 to 0.8 E_k
392 (4 Hz - 2 kHz), respectively. For carrot sprites, the E_s at the altitude of the brightest region
393 varied from 0.6 to 6.6 E_k (4 Hz to 400 kHz) and 0.03 to 1 E_k (4 Hz - 2 kHz), respectively.
394 This is in good agreement with Gamerota et al. (2011), Hu et al. (2007), Kanmae et al.
395 (2012), Li and Cummer (2012), and Qin et al. (2013).
396

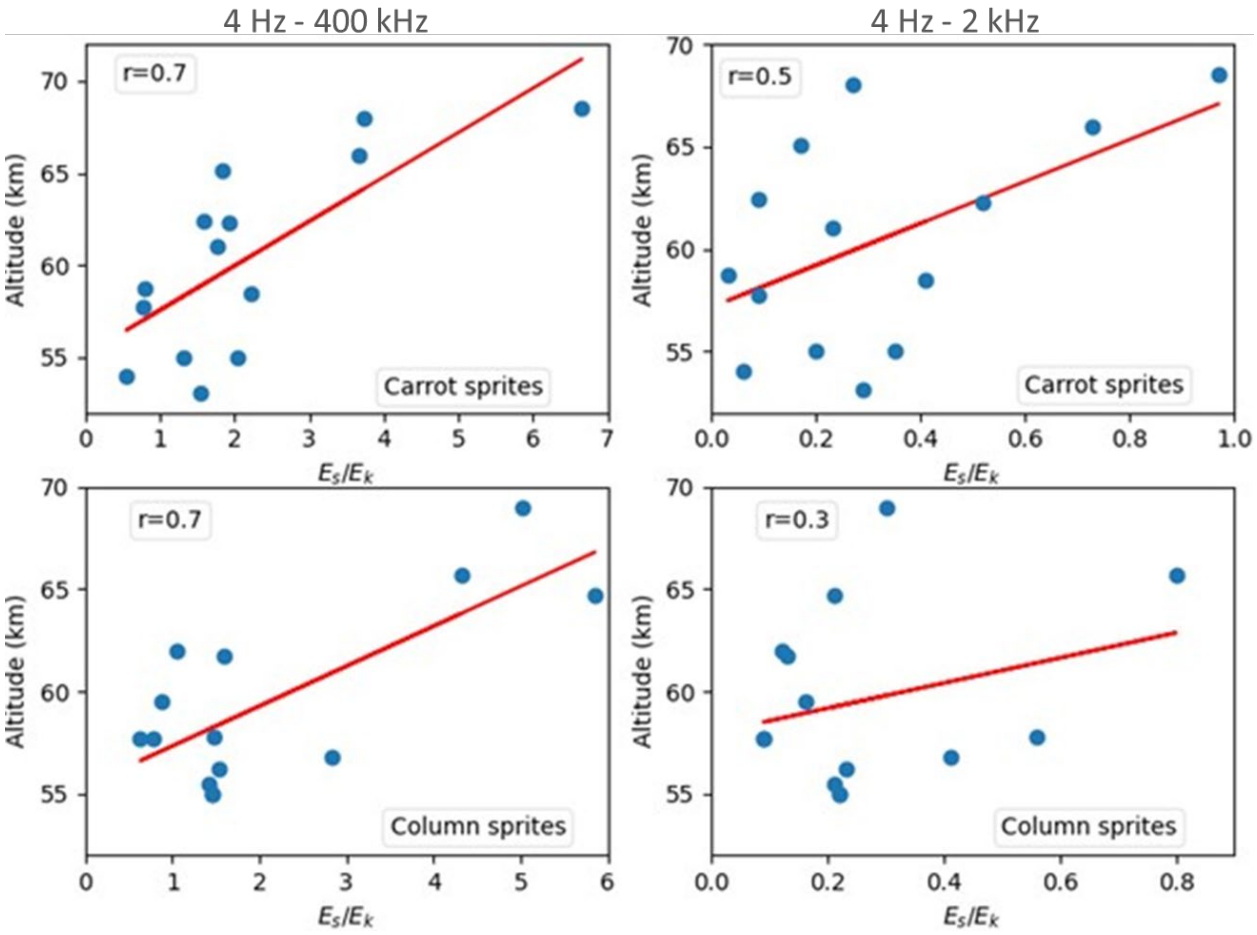

Figure 5. The relationship between the altitude/distance normalised lightning peak electric field over local air breakdown field (E_s/E_k) at the brightest region of column and carrot sprites versus atmospheric altitude. The lightning peak electric fields for the panels on the left panels were obtained in the frequency ranging from 4 Hz to 400 kHz, whereas the panels on the right were obtained in the frequency ranging from 4 Hz - 2 kHz.

Figure 5 shows relationship between the E_s/E_k at the brightest region of column and carrot sprites versus atmospheric altitude. A good linear correlation coefficient of 0.7 and 0.7 were found between E_s/E_k (4 Hz to 400 kHz) associated with column and carrot sprites' brightest region versus the brightest region altitude, respectively, see Figure 5 left panels. A good linear correlation coefficient of 0.5 was found between E_s/E_k (4 Hz - 2 kHz) associated with carrot sprites' brightest region versus the brightest region altitude, whereas a weak linear correlation coefficient of 0.3 was found for column sprites, see Figure 5 right panels. The weak correlation coefficient shows that the lightning return stroke at lower frequencies (4 Hz - 2 kHz) has less influence on the column sprites than on the carrot sprites formation processes.

From the 2020 data, the sprites events which occurred at 19:55:41.681 and 21:41:29.422 UTC had halos with diameters of about 65 and 61 km, respectively, see Tables 1 and 2. The E_s at the altitude of the brightest region of these events were 0.2 and 0.5 E_k (4 Hz to 400 kHz), and 0.1 and 0.4 E_k (4 Hz - 2 kHz), respectively. From the 2019 data, the sprites event which occurred at 19:41:09.728 UTC had a halo with diameter of about 57 km, see Table 3. The E_s at the altitude of the brightest region of this event were 1.5 E_k (4 Hz to 400 kHz) and 0.6 E_k (4 Hz - 2 kHz), respectively. An electric field value of greater than about 0.5 E_k has been associated with sprites halo discharge (Qin et al., 2013; Pasko et al., 2013). Note that halos were not seen by the camera with the red N_2 filter.

The photon flux and lightning initial peak Joule heating associated with the brightest region altitude of 14 column sprites were found to vary from 2.5×10^{-8} to 2.6×10^{-7} W/m^2 ($\pm2.4\times10^{-9}$ W/m^2) and 7.2×10^{-4} to 6.7×10^{-1} W/m^2 ($\pm6.2\times10^{-7}$ W/m^2), with an average value of approximately 8.4×10^{-8} W/m^2 and 7.5×10^{-2} W/m^2, respectively, for altitudes from 55 to 69 km. The photon flux and lightning peak Joule heating associated with 14 carrot sprites at the brightest region altitude ranged from 4.8×10^{-8} to 2.2×10^{-7} W/m^2 ($\pm2.6\times10^{-9}$ W/m^2) and 5.3×10^{-5} to 6.8×10^{-1} W/m^2 ($\pm4.3\times10^{-9}$ W/m^2) with an average value of approximately 1.3×10^{-7} W/m^2 and 9.4×10^{-2} W/m^2, respectively, for altitudes between 53 to 68.5 km. The value in parentheses is the uncertainty. The vertical extent of the brightest region for column and carrot sprites ranged from 0.6 to 2.2 km and 0.6 to 1.4 km, respectively.

To within the timing uncertainty of the video frame (±20 ms), we found that column and carrot sprites have a time delay that varied from about 18 to 27 ms and 30 to 145 ms from their parent lightning strokes, respectively. The time delay between the parent lightning strokes and column (< 30 ms) and carrot sprites (up to 145 ms) agrees with van der Velde et al. (2006). The sprite delay depends on the charge moment change in milliseconds (Cummer and Stanley, 1999).

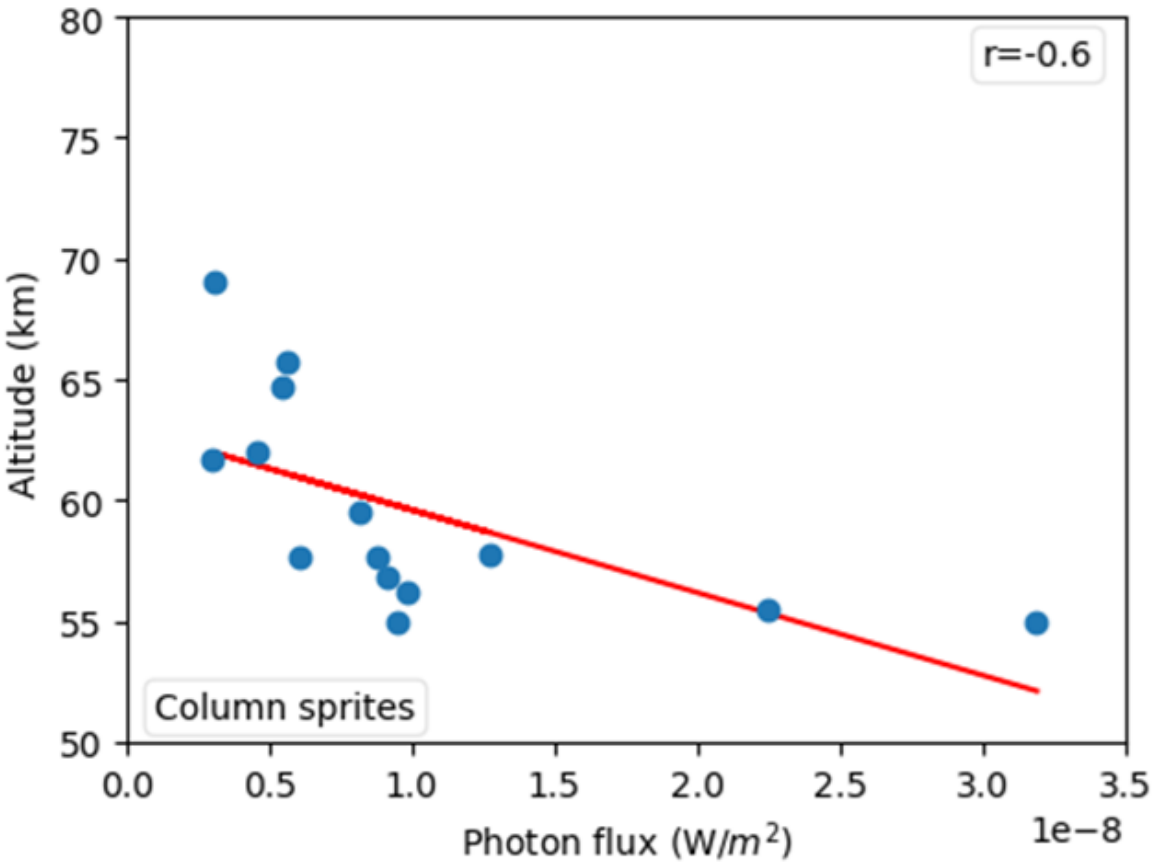

Figure 6. The relationship between the column sprite's photon flux versus sprite's brightest region altitude, respectively. r shows the linear correlation coefficient.

Figure 6 shows the column sprites' photon flux versus the sprites' brightest region altitude. r denotes the linear correlation coefficient. The photon flux out of column sprites' brightest region decreased with an increase in sprites' brightest region altitude, with a linear correlation coefficient of -0.6. The photon flux from carrot sprites' brightest region versus the brightest region altitude showed a weak positive correlation of 0.2 (not shown). A weak-moderate linear correlation coefficient of 0.4 and 0.3 was found between the altitude/distance normalised lightning initial peak Joule heating associated with column and carrot sprites' brightest region versus the brightest region altitude, respectively (not shown).

5. Conclusions

We have estimated the lightning peak apparent Poynting flux and peak initial Joule heating associated with the altitude of the brightest regions of sprites only. We investigated the lightning electric fields in the frequencies ranging from 4 Hz to 400 kHz and lightning return stroke at lower frequencies (4 Hz - 2 kHz). The E_s/E_k (0.1 to 6.6) values are comparable with

the sprites values from the published literature (Gamerota et al.,2011; Hu et al., 2007; Kanmae et al., 2012; Li and Cummer, 2012; Qin et al, 2013). The lightning discharges have an influence on carrot and column sprites formation processes. The lightning return stroke at lower frequencies (4 Hz - 2 kHz) has more influence on carrot sprites than on column sprites brightest region altitude.

From 2019, the averaged photon flux and lightning initial peak Joule heating associated with the brightest region of column sprites were found to be approximately 8.4×10^{-8} W/m^2 and 7.5×10^{-2} W/m^2, respectively, for altitudes from 55 to 69 km. The averaged photon flux and lightning initial peak Joule heating associated with the brightest region of carrot sprites were found to be approximately 1.3×10^{-7} W/m^2 and 9.4×10^{-2} W/m^2, respectively, for altitudes between 53 to 68.5 km. The column sprites' brightest region altitude had a linear correlation coefficient of -0.6 against the photon flux of the brightest region.

From 2020, the investigation of the altitude/distance normalised lightning peak apparent Poynting flux and initial peak Joule heating associated with the brightest region of sprites yield averaged energy fluxes of 12.7 W/m^2 and 4.7×10^{-3} W/m^2, respectively. A linear correlation coefficient of -0.7 was found between the peak apparent Poynting flux associated with the brightest region of sprites and atmospheric altitude, whereas a correlation coefficient of -0.4 was obtained between the initial peak Joule heating associated with the sprite's brightest region and atmospheric altitude. Our study shows for the first time that the apparent Poynting flux emanating from the sprite dominates over the Joule heating and photon flux by several orders of magnitude.

Our photon flux values are less than Armstrong et al. (1998) by up to 3 orders of magnitude. However, Armstrong et al. (1998) photon fluxes are also less than our Poynting flux and Joule heating of sprites and so consistent with our conclusion. Factors such as local clouds, viewing direction, spatial resolution, atmospheric scattering, light pollution, camera type and setting, distance to sprite, technical approach of measurements and humidity affects camera sensitivity, therefore sprites visibility (Mashao et al., 2022a; Mlynarczyk et al., 2015; Pasko et al., 2013).

6. Acknowledgements

DM, MK, and MF thank the South African National Space Agency, the University of KwaZulu-Natal, and the Royal Society (UK) grant NMG/R1/180252 for funding this work. DM, MK, and MF acknowledge the South African Lightning Detection Networks and Earth Networks Total Lightning Networks for supplying the lightning data. We thank Klara Anneliese Spieker for operating the camera system at the SAAO site in 2020.

7. References

Alekseeva, G. A., Arkharov, A. A., Galkin, V. D., Hagen-Thorn, E. I., Nikanorova, I. N., Novikov, V. V., ... and Shchegol, D. E. (1996). The Pulkovo Spectrophotometry Catalog of Bright Stars in the Range from 320 to 1080 Nm. *Open. Astron., 5*(4), pp.603-838. https://doi.org/10.1515/astro-1996-0401

Allied Vision. (2022). Retrieved 29 March 2022, from https://www.alliedvision.com/en/support/technical-documentation/pike-documentation.

Armstrong, R. A., Shorter, J. A., Taylor, M. J., Suszcynsky, D. M., Lyons, W. A., and Jeong, L. S. (1998). Photometric measurements in the SPRITES'95 and '96 campaigns of nitrogen second positive (399.8 nm) and first negative (427.8 nm) emissions. *J. Atmos. Sol. Terr. Phys., 60*(7-9), 787-799. https://doi.org/10.1016/S1364-6826(98)00026-1

Asano, T., Hayakawa, M., Cho, M., and Suzuki, T. (2008). Computer simulations on the initiation and morphological difference of Japan winter and summer sprites. *J. Geophys. Res. Space. Phys.*, *113*(A2). https://doi.org/10.1029/2007ja012528

Bór, J. (2013). Optically perceptible characteristics of sprites observed in Central Europe in 2007–2009. *J. Atmos. Sol. Terr. Phys.,* 92, pp.151-177. https://doi.org/10.1016/j.jastp.2012.10.008

Bór, J., André, K. S., Bozóki, T., Mlynarczyk, J., Steinbach, P., Novák, A., and Lemperger, I. (2022). Estimating the Attenuation of ELF-band Radio Waves in the Earth's Crust by Q-bursts. *IEEE Trans. Antennas. Propag., 70*(8). pp. 6973-6982. https://doi.org/10.1109/TAP.2022.3161504

Bui, V., Chang, L. C., and Heckman, S. (2015, December). A performance study of earth networks total lighting network (ENTLN) and worldwide lightning location network (WWLLN). In 2015 International Conference on Computational Science and Computational Intelligence (CSCI) (pp. 386-391). IEEE. https://doi.org/10.1109/csci.2015.120

524 Constable, C. (2016). Earth's electromagnetic environment. *Surv Geophys, 37*(1), 27-45.
525 https://doi:10.1007/s10712-015-9351-1.

526 Cooray, V., and Lobato, A. (2020). The Energy, Momentum, and Peak Power Radiated by
527 Negative Lightning Return Strokes. Atmosphere, 11(12), 1288.
528 https://doi.org/10.3390/atmos11121288

529 Cummer, S.A. and Stanley, M., 1999. Submillisecond resolution lightning currents and sprite
530 development: Observations and implications. *Geophys. Res. Lett., 26*(20), pp.3205-3208.
531 https://doi.org/10.1029/1999GL003635

532 Cummer, S. A., Lyons, W. A., and Stanley, M. A. (2013). Three years of lightning impulse
533 charge moment change measurements in the United States. *J. Geophys. Res. Atmos, 118*(11),
534 5176-5189, doi:10.1002/jgrd.50442.

535 Dowden, R. L., Rodger, C. J., and Nunn, D. (2001). Minimum sprite plasma density as
536 determined by VLF scattering. *IEEE Trans. Antennas Propag., 43*(2), 12-24. doi:
537 10.1109/74.924600.

538 Earthnetworks.com. (2020). Retrieved 24 January 2020, from
539 https://www.earthnetworks.com/product/decision-support-collaboration-tools/sferic-maps/.

540 Farrell, W. M., Goldberg, R. A., Blakeslee, R. J., Desch, M. D., and Mach, D. M. (2006).
541 Radiation impedance over a thunderstorm. *Radio. Sci., 41*(03), 1-7. https://doi:
542 10.1029/2004RS003217

543 Foster, J. C., St.-Maurice, J. P., and Abreu, V. J. (1983). Joule heating at high latitudes. *J.*
544 *Geophys. Res. Space. Phys., 88*(A6), 4885-4897. https://doi.org/10.1029/JA088iA06p04885

545 Franz, R. C., Nemzek, R. J., and Winckler, J. R. (1990). Television image of a large upward
546 electrical discharge above a thunderstorm system. *Sci., 249*(4964), 48-51.
547 https://doi.org/10.1126/science.249.4964.48

548 Fraser-Smith, A. C., and Bowen, M. M. (1992). The natural background levels of 50/60 Hz
549 radio noise. *IEEE Transactions on Electromagnetic compatibility, 34*(3), 330-337. https://doi:
550 10.1109/15.155849.

551 Füllekrug, M. (2006). Elementary model of sprite igniting electric fields. *Am. J. Phys., 74*(9),
552 804-805. https://doi.org/10.1119/1.2206573.

553 Füllekrug, M., Ignaccolo, M., and Kuvshinov, A. (2006). Stratospheric Joule heating by
554 lightning continuing current inferred from radio remote sensing, *Radio Sci, 41*(02), 1-5,
555 RS2S19. https://doi:10.1029/2006RS003472.

556 Füllekrug, M. (2010). Wideband digital low-frequency radio receiver. *Meas. Sci. Technol.,*
557 *21*(1), p.015901. https://doi.org/10.1088/0957-0233/21/1/015901

558 Füllekrug, M., Nnadih, S., Soula, S., Mlynarczyk, J., Stock, M., Lapierre, J., and Kosch, M.
559 (2019). Maximum sprite streamer luminosity near the Stratopause. *Geophys. Res.*
560 *Lett., 46*(21), pp.12572-12579. https://doi.org/10.1029/2019GL084331

561 Gamerota, W. R., Cummer, S. A., and Li, J. (2011). Comparison of sprite initiation altitudes
562 between observations and models. *J. Geophys. Res. Space. Phys., 116*(A2).
563 https://doi.org/10.1029/2010JA016095

564 Gijben, M. (2012). The lightning climatology of South Africa. *S. Afri. J. Sci., 108*(3), pp.1-
565 10. https://doi.org/10.4102/sajs.v108i3/4.740

566 Gomez Kuri, Z., Soula, S., Neubert, T., Mlynarczyk, J., and Köhn, C. (2021). Converging
567 Luminosity in Column-Sprite Filaments. *Geophys. Res. Lett., 48*(6), e2020GL090364.
568 https://doi.org/10.1029/2020GL090364

569 Gordillo-Vázquez, F. J., & Luque, A. (2010). Electrical conductivity in sprite streamer
570 channels. *Geophys. Res. Lett., 37*(16). https://doi.org/10.1029/2010GL044349

571 Gordillo-Vázquez, F. J., Passas, M., and Luque, A., (2018). High spectral resolution
572 spectroscopy of sprites: A natural probe of the mesosphere. *J. Geophys. Res. Atmos., 123*(4),
573 2336-2346. https://doi.org/10.1002/2017JD028126

574 Hampton, D. L., Heavner, M. J., Wescott, E. M., and Sentman, D. D. (1996). Optical spectral
575 characteristics of sprites. *Geophys. Res. Lett., 23*(1), 89-92.
576 https://doi.org/10.1029/95GL03587

577 Heavner, M. J., Morrill, J. S., Siefring, C., Sentman, D. D., Moudry, D. R., Wescott, E. M.,
578 and Bucsela, E. J. (2010). Near-ultraviolet and blue spectral observations of sprites in the
579 320–460 nm region: N_2 (2PG) emissions. *J. Geophys. Res. Space. Phys., 115*(A7).
580 https://doi.org/10.1029/2009JA014858

Hu, W., Cummer, S. A., and Lyons, W. A. (2007). Testing sprite initiation theory using lightning measurements and modeled electromagnetic fields. *J. Geophys. Res. Atmos., 112*(D13). https://doi.org/10.1029/2006JD007939

Kanmae, T., Stenbaek-Nielsen, H. C., and McHarg, M. G. (2012). Diameter-speed relation of sprite streamers. *J. Phys. D: Appl Phys., 45*(27), 275203. https://doi.org/10.1088/0022-3727/45/27/275203

Kitagawa, N., Brook, M., and Workman, E. J. (1962). Continuing currents in cloud-to-ground lightning discharges. *J. Geophys. Res., 67*(2), 637-647. https://doi.org/10.1029/JZ067i002p00637

Kosch, M. J., and Nielsen, E. (1995). Coherent radar estimates of average high-latitude ionospheric Joule heating. *J. Geophys. Res. Space. Phys., 100*(A7), pp.12201-12215. https://doi.org/10.1029/95ja00821

Kuo, C. L., Chou, J. K., and Tsai, L. Y. (2009). Discharge processes, electric field, and electron energy in ISUAL-recorded gigantic jets. *J. Geophys. Res. Space. Phys., 114*(A4). https://doi.org/10.1029/2008JA013791

Li, J., Cummer, S. A., Lyons, W. A., and Nelson, T. E. (2008). Coordinated analysis of delayed sprites with high-speed images and remote electromagnetic fields. *J. Geophys. Res. Atmos.*, *113*(D20). https://doi.org/10.1029/2008JD010008

Li, J., and Cummer, S. (2012). Relationship between sprite streamer behavior and lightning-driven electric fields. *J. Geophys. Res. Space. Phys., 117*(A1). https://doi.org/10.1029/2011JA016843

Liu, N., Pasko, V.P., and Frey, H.U. (2009a). Assessment of sprite initiating electric fields and quenching altitude of $a^1\Pi_g$ state of N_2 using sprite streamer modeling and ISUAL spectrophotometric measurements. *J. Geophys. Res. Space. Phys., 114*(A3). https://doi.org/10.1029/2008JA013735

Liu, N. Y., Pasko, V. P., and Adams, K. (2009b), Comparison of acceleration, expansion, and brightness of sprite streamers obtained from modeling and high-speed video observations. *J. Geophys. Res., 114*, A00E03. doi: 10.1029/2008JA013720

Liu, N., McHarg, M. G., and Stenbaek-Nielsen, H. C. (2015). High-altitude electrical discharges associated with thunderstorms and lightning. *J. Atmos. Sol. Terr. Phys.*, *136*, pp.98-118. https://doi.org/10.1016/j.jastp.2015.05.013

Luque, A., and Ebert, U. (2009). Emergence of sprite streamers from screening-ionisation waves in the lower ionosphere. *Nat. Geosci., 2*(11), 757-760. https://doi.org/10.1038/ngeo662

Luque, A. and Ebert, U, (2010). Sprites in varying air density: Charge conservation, glowing negative trails and changing velocity. *Geophys. Res. Lett., 37*(6). https://doi.org/10.1029/2009GL041982

Luque, A., and Gordillo-Vázquez, F. J. (2012). Mesospheric electric breakdown and delayed sprite ignition caused by electron detachment. *Nat. Geosci., 5*(1), 22-25. https://doi.org/10.1038/ngeo1314

Luque, A., Stenbaek-Nielsen, H. C., McHarg, M. G., and Haaland, R. K. (2016). Sprite beads and glows arising from the attachment instability in streamer channels. *J. Geophys. Res. Space. Phys.*, *121*(3), pp.2431-2449. https://doi.org/10.1002/2015ja022234

Malagón-Romero, A., Teunissen, J., and Stenbaek-Nielsen, H. C. (2020). On the emergence mechanism of carrot sprites. *Geophys. Res. Lett.*, *47*(1), p.e2019GL085776. https://doi.org/10.1029/2019GL085776

Mashao, D. C., Kosch, M. J., Bór, J., and Nnadih, S. (2021). The altitude of sprites observed over South Africa. *S. Afri. J. Sci.*, *117*(1-2), pp.1-8. https://doi.org/10.17159/sajs.2021/7941

Mashao, D., Kosch, M., Fullekrug, M., and Ivchenko, M. (2022a). 3D triangulation of transient luminous events over Africa. *Adv. Space. Res.* https://doi.org/10.1016/j.asr.2022.08.057

Mashao, D. C., Kosch, M. J., Füllekrug, M., and Mlynarczyk, J. (2022b). Lightning parameters of sprites and diameter of halos over South Africa. *J. Atmos. Sol. Terr. Phys.*, *105957*. https://doi.org/10.1016/j.jastp.2022.105957

McHarg, M. G., Stenbaek-Nielsen, H. C., and Kammae, T. (2007). Observations of streamer formation in sprites. *Geophys. Res. Lett., 34*(6). https://doi.org/10.1029/2006GL027854

Mende, S. B., Rairden, R. L., Swenson, G. R., and Lyons, W. A. (1995). Sprite spectra; N_2 1 PG band identification. *Geophys. Res. Lett., 22*(19), 2633-2636. https://doi.org/10.1029/95GL02827

639 Mlynarczyk, J., Bo´r, J., Kulak, A., et al., (2015). An unusual sequence of sprites followed by
640 a secondary TLE: An analysis of ELF radio measurements and optical observations. *J.*
641 *Geophys. Res. Space Phys.120* (3), 2241–2254. https://doi.org/10.1002/2014ja020780

642 Nnadih, S., Kosch, M., Martinez, P., and Bor, J. (2018). First ground-based observations of
643 sprites over southern Africa. *S. Afri. J. Sci., 114*(9-10), 1-6.
644 http://dx.doi.org/10.17159/sajs.2018/4272

645 Nnadih, S., Kosch, M., and Mlynarczyk, J. (2021). Estimating the electron energy and the
646 strength of the electric field within sprites using ground-based optical data observed over
647 South African storms. *J. Atmos. Sol. Terr. Phys., 225*, p.105760.
648 https://doi.org/10.1016/j.jastp.2021.105760

649 Pasko, V. P. (2010). Recent advances in theory of transient luminous events. *J. Geophys. Res.*
650 *Space. Phys., 115*(A6). https://doi.org/10.1029/2009JA014860

651 Pasko, V. P., Qin, J., and Celestin, S. (2013). Toward better understanding of sprite
652 streamers: initiation, morphology, and polarity asymmetry. *Surv. Geophys., 34*(6), 797-830.
653 https://doi.org/10.1007/s10712-013-9246-y

654 Qin, J., Celestin, S., and Pasko, V. P. (2013). Dependence of positive and negative sprite
655 morphology on lightning characteristics and upper atmospheric ambient conditions. *J.*
656 *Geophys. Res. Space. Phys., 118*(5), 2623-2638. https://doi.org/10.1029/2012JA017908

657 Ren, H., Lu, G., Cummer, S. A., Peng, K. M., Lyons, W. A., Liu, F., ... and Cheng, Z. (2021).
658 Comparison between high-speed video observation of sprites and broadband sferic
659 measurements. *Geophys. Res. Lett., 48*(10), e2021GL093094.
660 https://doi.org/10.1029/2021GL093094

661 Sentman, D. D., Wescott, E. M., Osborne, D. L., Hampton, D. L., and Heavner, M. J. (1995).
662 Preliminary results from the Sprites94 aircraft campaign: 1. Red sprites. *Geophys. Res. Lett.,*
663 *22*(10), 1205-1208. https://doi.org/10.1029/95GL00583

664 Shibusawa, K., and Funatsu, M. (2019). Radiative Characteristics of N_2 First Positive Band in
665 Visible and Near-infrared Regions for Microwave-discharged Nitrogen Plasma. *Trans. Jpn.*
666 *Soc. Aeronaut. Space Sci., 62*(2), 86-92. https://doi.org/10.2322/tjsass.62.86

667 Stenbaek-Nielsen, H. C., and McHarg, M. G. (2008). High time-resolution sprite imaging:
668 observations and implications. *J. Phys. D. Appl. Phys., 41*(23), 234009.
669 https://doi.org/10.1088/0022-3727/41/23/234009

670 Stenbaek-Nielsen, H. C., Haaland, R., and McHarg, M. G. (2010). Sprite initiation altitude
671 measured by triangulation. *J. Geophys. Res. Space. Phys., 115*(A3).
672 https://doi.org/10.1029/2009ja014543

673 Surkov, V. V., and Hayakawa, M. (2012, August). Underlying mechanisms of transient
674 luminous events: a review. In *Ann. Geophys.,* (Vol. 30, No. 8, pp. 1185-1212). Copernicus
675 GmbH. https://doi.org/10.5194/angeo-30-1185-2012

676 Surkov, V. V., and Hayakawa, M. (2020). Progress in the study of transient luminous and
677 atmospheric events: A review. *Surv. Geophys., 41*(5), 1101-1142.
678 https://doi.org/10.1007/s10712-020-09597-2

679 Suszcynsky, D. M., Roussel-Dupré, R., Lyons, W. A., and Armstrong, R. A. (1998). Blue-
680 light imagery and photometry of sprites. *J. Atmos. Sol. Terr. Phys., 60*(7-9), 801-809.
681 https://doi.org/10.1016/S1364-6826(98)00027-3

682 Taylor, W. L., and Jean, A. G. (1959). Very-low-frequency radiation spectra of lightning
683 discharges. NBS *J. Res. Radio. Propagation., 63*(2), 199.
684 https://doi.org/10.6028/jres.063d.021

685 Tomicic, M., Soula, S., Defer, E., Prieur, S., Mlynarczyk, J., Farges, T., ... and Neubert, T.
686 (2021). Dancing Sprites Above a Lightning Mapping Array—An Analysis of the Storm and
687 Flash/Sprite Developments. *J. Geophys. Res. Atmos., 126*(20), e2021JD035059.
688 https://doi.org/10.1029/2021JD035059

689 van der Velde, O. A., Mika, Á., Soula, S., Haldoupis, C., Neubert, T., and Inan, U. S. (2006).
690 Observations of the relationship between sprite morphology and in-cloud lightning processes.
691 *J. Geophys. Res. Atmos., 111*(D15). https://doi.org/10.1029/2005JD006879

692 Wescott, E. M., Sentman, D. D., Heavner, M. J., Hampton, D. L., Lyons, W. A., and Nelson,
693 T. (1998). Observations of 'Columniform'sprites. *J. Atmos. Sol. Terr. Phys., 60*(7-9), 733-
694 740. https://doi.org/10.1016/s1364-6826(98)00029-7

695 Wescott, E. M., Stenbaek-Nielsen, H. C., Sentman, D. D., Heavner, M. J., Moudry, D. R.,
696 and Sabbas, F. S. (2001). Triangulation of sprites, associated halos and their possible relation

697 to causative lightning and micrometeors. *J. Geophys. Res. Space. Phys., 106*(A6), pp.10467-
698 10477. https://doi.org/10.1029/2000ja000182

699 Worthpoint. (2022). Retrieved 29 March 2022, from
700 https://www.worthpoint.com/worthopedia/mullard-phillips-photonis-xx1332-gen-510751285.

701 Zhu, Y., Rakov, V. A., Tran, M. D., Stock, M. G., Heckman, S., Liu, C., ... and Hare, B. M.
702 (2017). Evaluation of ENTLN performance characteristics based on the ground truth natural
703 and rocket-triggered lightning data acquired in Florida *J. Geophys. Res. Atmos., 122*(18),
704 pp.9858-9866. https://doi.org/10.1002/2017JD027270

Appendix

Table 1: Summary of estimations of lightning peak apparent Poynting flux at the brightest region altitude of sprites observed from SKA and SAAO sites on 24 January 2020. All CG lightning events are of positive polarity. E_s is the electric field at sprite's brightest region altitude.

Time (UT)	Lightning peak current (kA)	Distance from the receiver to the lightning stroke (km)	Sprite's brightest region altitude (km)	Azimuth angle from the magnetic coil to the lightning stroke (°)	Adjusted Magnetic field at receiver (T)	Magnetic field at 1 km from lightning location (T)	Electric field at 1 km from lightning location (V/m)	N_2 density at sprite's brightest region altitude (cm^{-3})	Electric field at sprite's brightest region altitude (E_s) (V/m)	Magnetic field at sprite's brightest region altitude (T)	Lightning peak apparent Poynting flux at sprite's brightest region altitude (W/m^2)	Es/E_k 4 Hz to 400 kHz	Es/E_k 4 Hz - 2 kHz
19:55:41.682 (SKA)	142	389.9	61.5	99.1	1.8E-09	2.8E-04	7.1E+03	4.4E+15	3.1E+01	1.2E-06	29.3	0.2	0.1
20:00:54.029 (SKA)	101	390.1	61.7	101.1	1.1E-09	1.6E-04	5.4E+03	4.4E+15	2.3E+01	7.0E-07	12.8	0.2	0.04
20:03:13.971 (SKA)	74	431.9	74.2	93.8	5.6E-10	1.0E-04	1.1E+03	8.1E+14	2.8E+00	2.6E-07	0.6	0.1	0.03
20:03:14.307 (SKA)	62	417.9	75.3	101.7	3.0E-10	5.3E-05	4.5E+02	6.9E+14	1.1E+00	1.2E-07	0.1	0.1	0.01
20:07:29.608 (SKA)	92	403.0	72.0	98.9	8.2E-10	1.3E-04	3.0E+03	1.1E+15	8.1E+00	3.6E-07	2.3	0.3	0.1
20:07:29.248 (SKA)	127	449.6	71.0	108.6	1.2E-09	2.3E-04	8.9E+03	1.3E+15	2.5E+01	6.5E-07	12.8	0.5	0.2
20:23:43.573 (SAAO)	66	562.3	68.2	30.9	2.0E-09	6.3E-04	6.0E+03	1.9E+15	1.9E+01	2.0E-06	30.1	0.3	0.1
21:41:29.422 (SKA)	133	209.5	71.4	159.1	2.1E-09	9.2E-05	2.5E+04	1.3E+15	6.9E+01	2.5E-07	13.8	0.5	0.4

Table 2: Summary of estimations of lightning peak initial Joule heating associated with the brightest region altitude of sprites observed from SKA and SAAO sites on 24 January 2020. All CG lightning events are of positive polarity. E_s is the electric field at sprite's brightest region altitude.

Time (UT)	Lightning peak current (kA)	Distance from the receiver to the lightning stroke (km)	Electric field at 1 km from lightning location (V/m)	Sprite's brightest region altitude (km)	Atmospheric conductivity (S/m)	Sprites brightest region vertical extent (km)	Electric field at sprite's brightest region altitude (E_s) (V/m)	Lightning peak initial Joule heating at the sprite's brightest region altitude (W/m^2)
19:55:41.682 (SKA)	142	389.9	7.1E+03	61.5	8.0E-09	1.3	3.1E+01	9.6E-03
20:00:54.029 (SKA)	101	390.1	5.4E+03	61.7	8.0E-09	1.3	2.3E+01	5.6E-03
20:03:13.971 (SKA)	74	431.9	1.1E+03	74.2	1.0E-08	1.5	2.8E+00	1.1E-04
20:03:14.307 (SKA)	62	417.9	4.5E+02	75.3	1.0E-08	2.3	1.1E+00	2.6E-05
20:07:29.608 (SKA)	92	403.0	3.0E+03	72.0	9.8E-08	2.2	8.1E+00	1.4E-02
20:07:29.248 (SKA)	127	449.6	8.9E+03	71.0	1.0E-09	2.4	2.5E+01	1.5E-03
20:23:43.573 (SAAO)	66	562.3	6.0E+03	68.2	3.0E-09	1.4	1.9E+01	1.5E-03
21:41:29.422 (SKA)	133	209.5	2.5E+04	71.4	1.0E-09	1.2	6.9E+01	5.8E-03

Table 3: Summary of estimations of photon flux and lightning peak initial Joule heating at the brightest region of column sprites observed from the SKA site on 01 February 2019. All CG lightning events are of positive polarity. E_s is the electric field at sprite's brightest altitude.

Time (UT)	Lightning peak current (kA)	Distance from the receiver to the lightning stroke (km)	Sprites photon fluxes (W/m^2)	Sprite's brightest region altitude (km)	Sprite's brightest region vertical extent (km)	N_2 density at sprite's brightest region altitude (cm^{-3})	Electric field at sprite's bright region altitude (ELF/VLF/LF radio receiver) (E_s) (V/m)	Lightning peak initial Joule heating at the sprite's brightest region altitude (W/m^2)	Es/E_k 4 Hz to 400 kHz	Es/E_k 4 Hz - 2 kHz
19:05:21.584	50	357.3	2.7E-07	55.0	1.1	1E+16	263.5	1.6E-02	1.4	0.2
19:05:21.584	50	357.3	1.9E-07	55.5	1.1	1E+16	256.4	1.5E-02	1.4	0.2
19:05:21.584	50	357.3	8.0E-08	55.0	1.1	1E+16	263.5	1.6E-02	1.4	0.2
19:05:21.584	50	357.3	8.3E-08	56.2	1.1	9E+15	246.9	1.4E-02	1.5	0.2
19:06:49.098	107	360.4	7.7E-08	56.8	0.6	8E+15	399.0	1.9E-02	2.8	0.4
19:35:00.707	80	334.4	4.7E-08	65.7	2.2	2.6E+15	248.1	6.7E-01	0.8	4.3
19:43:09.728	103	333.6	1.1E-07	57.8	1.1	7.1E+15	479.6	2.5E-02	1.5	0.6
19:47:59.520	64	332.1	6.9E-08	59.5	1.1	6.3E+15	124.6	1.5E-01	0.9	0.2
19:56:54.499	28	345	5.1E-08	57.7	1.1	7.1E+15	80.3	7.2E-04	0.8	0.1
19:56:54.499	28	345	7.4E-08	57.7	1.1	7.1E+15	80.3	7.2E-04	0.6	0.1
19:56:54.499	28	345	3.9E-08	62.0	1.1	4.4E+15	64.7	3.7E-02	1.0	0.1
19:56:54.499	28	345	2.5E-08	61.7	1.1	4.4E+15	65.7	3.8E-02	1.6	0.1
20:12:08.503	41	436.9	2.6E-08	69.0	1.4	1.7E+15	59.9	1E-02	5.0	0.3
20:12:08.503	41	436.9	4.6E-08	64.7	1.4	2.9E+15	72.9	3.7E-02	5.8	0.2

Table 4: Summary of estimations of photon flux and lightning peak initial Joule heating at the brightest region of carrot sprites observed from the SKA site on 01 February 2019. All CG lightning events are of positive polarity. E_s is the electric field at sprite's brightest region altitude.

Time (UT)	Lightning peak current (kA)	Distance from the receiver to the lightning stroke (km)	Sprites photon fluxes (W/m^2)	Sprite's brightest region altitude (km)	Sprites brightest region vertical extent (km)	N_2 density at sprite's brightest region altitude (cm^{-3})	Electric field at sprites bright region altitude (ELF/VLF/LF radioreceiver) (E_s) (V/m)	Lightning peak initial Joule heating at the sprite's brightest region altitude (W/m^2)	Es/E_k 4 Hz to 400 kHz	Es/E_k 4 Hz - 2 kHz
19:06:49.098	107	360.4	1.7E-07	68.5	0.6	2E+15	227.5	9.4E-02	6.7	1
19:08:24.111	92	309.1	1.5E-07	66.0	0.7	2.6E+15	225.2	1.7E-01	3.7	0.7
19:12:42.451	62	351.3	8.6E-08	62.3	1.1	4.4E+15	273.7	6.8E-01	1.9	0.5
19:26:48.376	42	333.1	2.0E-07	65.1	1.1	3E+15	60.7	2.0E-02	1.8	0.2
19:35:00.707	80	334.4	2.2E-07	58.5	1.1	7.1E+15	351.5	1.3E-02	2.2	0.4
19:36:23.568	42	409.4	1.2E-07	55.0	0.9	1E+16	238.1	9.9E-03	1.3	0.2
19:44:48.189	31	338.9	6.9E-08	54.0	0.7	1.1E+16	76.8	8.5E-04	0.6	0.1
19:49:30.929	49	345.9	1.5E-07	61.0	1.1	4.9E+15	136.5	1.7E-01	1.8	0.2
19:51:17.824	29	332	1.3E-07	58.7	1.1	6.3E+15	22.3	5.3E-05	0.8	0.03
19:53:59.597	48	413.9	7.3E-08	62.4	1.3	4.4E+15	46.4	2.3E-02	1.6	0.1
19:56:54.499	28	345	1.5E-07	57.7	1.1	7.1E+15	80.3	7.2E-04	0.8	0.1
19:57:34.604	92	352.4	2.0E-07	55.0	1.1	1E+16	425.7	4.1E-02	2	0.4
20:12:08.503	41	436.9	1.0E-07	68.0	1.4	1.9E+15	62.6	1.7E-02	3.7	0.3
20:38:25.718	68	431.6	4.8E-08	53.0	1.4	1.3E+16	438	8.0E-02	1.5	0.3

Poynting flux estimation calculation

The lightning peak apparent Poynting flux associated with the sprite's brightest region altitude calculation is demonstrated below using the sprites event in Figure 2. The lightning electric field (**E**) and magnetic field at the receivers' location were observed to be 3.6×10^{-2} V/m and 1.06×10^{-9} T, respectively (see Figure 2). The lightning discharge which initiates the sprites event was located 390.1 km away from the receivers' location. The sprite's brightest region altitude was 61.7 km. We only recorded the dominant horizontal component of the magnetic field due to technical issues with the second orthogonal induction coil. We first determine the azimuth angle from the magnetic coil to the lightning stroke in order to calculate the total horizontal magnetic field ($\mathbf{B_T}$) using Equation (A1) below:

$$\mathbf{B_T} = \mathbf{B}/\sin(AZ) \qquad (1A)$$

where *AZ* is the azimuth angle between the lightning position and the North-South coil orientation. *AZ* was found to be 101.1°. By using Equation (A1), we obtain $\mathbf{B_T} = 1.08 \times 10^{-9}$ T.

To normalise **E** and $\mathbf{B_T}$ values to 1 km from the lightning location, we then multiply **E** and $\mathbf{B_T}$ values by the distance (390.1 km) squared in km. We found **E** and $\mathbf{B_T}$ at 1 km from the lightning location to be:

$\mathbf{E} = 5.4 \times 10^{3}$ V/m

$\mathbf{B_T} = 1.6 \times 10^{-4}$ T

Assuming that the CG lightning charges, which initiated the sprites events, were removed at 10 km altitude, we then project **E** and $\mathbf{B_T}$ at 1 km from the lightning location to the sprite's brightest region altitude (61.7 km) by multiplying **E** and $\mathbf{B_T}$ at 1 km from the lightning location by $(10/r)^3$, where *r* is the altitude (km) of the sprite's brightest region (*r* = 61.7). We obtained **E** and $\mathbf{B_T}$ at the sprite's brightest region altitude to be:

$\mathbf{E} = 2.3 \times 10^{1}$ V/m

$\mathbf{B_T} = 7.0 \times 10^{-7}$ T

Finally, we estimated the lightning peak apparent Poynting flux (**S**) associated with the sprite's brightest region altitude using Equation (A2) below:

$$\mathbf{S} = \frac{(\mathbf{E} \times \mathbf{B})}{\mu} \quad \text{(A2)}$$

where μ is the permeability of the medium (assumed vacuum). For the event in Figure 2, we found that **S** = 12.8 W/m^2. This calculation is summarised in Table 1 (row 3).

Joule heating estimation calculation

The lightning peak initial Joule heating associated with the sprite's brightest region altitude calculation is demonstrated below using the sprites event in Figure 2. The lightning electric field (**E**) at the receiver's location was obtained to be 3.6×10^{-2} V/m (see Figure 2a). The lightning discharge which initiates the sprites event was located 390.1 km away from the receiver's location. The sprite's brightest region altitude was 61.7 km.

To normalise the **E** value to 1 km from the lightning location, we then multiply the **E** value by the distance (390.1 km) squared in km. We found **E** at 1 km from the lightning location to be:

$$\mathbf{E} = 5.4 \times 10^{3} \text{ V/m}$$

Assuming that the CG lightning charges, which initiated the sprites events, were removed at 10 km altitude, we then project **E** at 1 km from the lightning location to the sprite's brightest region altitude (61.7 km) by multiplying **E** at 1 km from the lightning location by $(^{10}/_{r})^{3}$, where *r* is the altitude (km) of the sprite's brightest region (*r* = 61.7). We obtained **E** at the sprite's brightest region altitude to be:

$$\mathbf{E} = 2.3 \times 10^{1} \text{ V/m}$$

We adopted the atmospheric conductivity (**σ**) from Lui et al. (2015), integrated over the vertical extent of the brightest region altitude of the sprite. The vertical extent of the brightest region altitude of sprite was found to be 1.3 km, and the corresponding **σ** was found to be:

$$\boldsymbol{\sigma} = 8 \times 10^{-9} \text{ S/m}$$

To determine the lightning peak initial Joule heating ($\mathbf{J_h}$) associated with the sprite's brightest region altitude, we used Equation (A3) below:

$$\mathbf{J_h} = \boldsymbol{\sigma}\mathbf{E}^2 \quad \text{(A3)}$$

For the event in Figure 2, we found that $\mathbf{J_h} = 5.6 \times 10^{-3}$ W/m^2. This calculation is summarised in Table 2 (row 3).

Photon flux estimation calculation

To determine the photon flux out of the sprite's brightest region, we acquired sprites optical data observed with a red N_2 emission filter (https://www.schott.com/shop/advanced-optics/en/Matt-Filter-Plates/RG645/c/glass-RG645) simultaneously with calibrated stars of known photon flux, as described in Nnadih et al. (2021). The flux values of selected stars can be found in the Pulkovo Spectrophotometry Bright Stars Catalogue (Alekseeva et al., 1996). We demonstrate how we determine the photon flux out of the sprite's brightest region using the sprites event in Figure 3. We averaged the sprites video clip frames over one second in order to determine the average intensity pixel value of the calibrated star ($\mathrm{Str_{avg}}$). The sky background ($\mathrm{Sky_{bkg}}$) value was obtained by using a 7×7 median filter to remove the stars on the video frame prior to the frame which contains the sprites event. The sky background ($\mathrm{Sky_{bkg}}$) value was 3. The calibrated star in Figure 3 was recorded using cameras with red N_2 emission filter that has an absolute photon flux ($\mathrm{Str_{flux}}$) of 0.32058 W/m^2. The photon flux value of the calibrated star was integrated over the filter's longpass wavelength range, see Figure A1. The calibrated star ($\mathrm{Str_{avg}}$) observed with red N_2 emission filter had an average intensity pixel value of 17.1. We average the image pixel values at the sprite's brightest region altitude in order to determine the sprite's average brightness ($\mathrm{Sprs_{avg}}$). The $\mathrm{Sprs_{avg}}$ in Figure 3 had a pixel intensity value of 65.

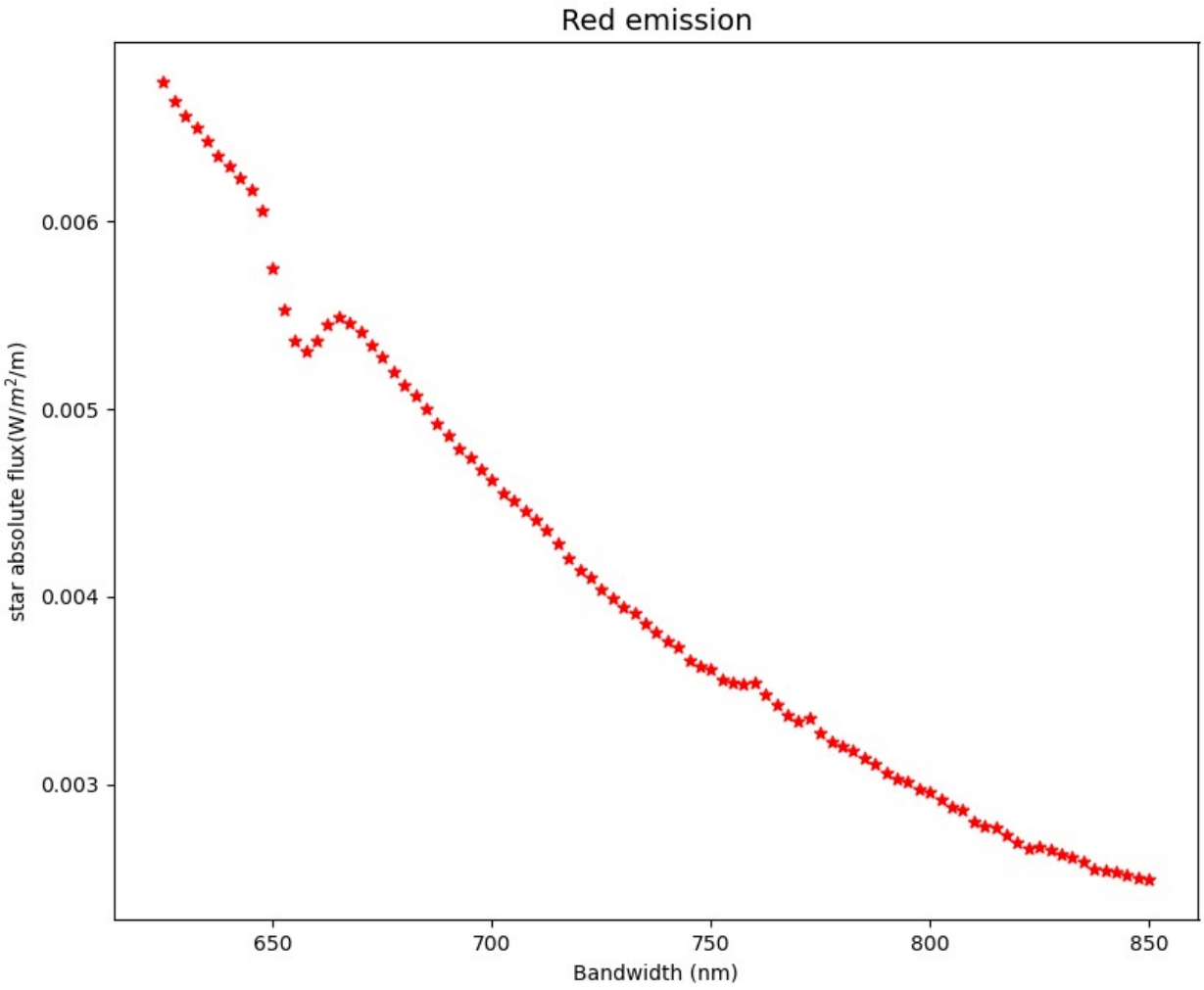

Figure A1. The calibrated star's absolute photon flux over the $N_2{}^1P$ emission range (Alekseeva et al., 1996).

We used data from the camera with a red filter to obtain the photon flux at the sprite's brightest region ($Sprs_{flux}$= 1.7×10^{-7} W/m^2), by means of Equation (4) (Nnadih et al., 2021).

$$Sprs_{flux} = \frac{Str_{flux}(Sprs_{avg} - Sky_{bkg})}{Str_{avg} - Sky_{bkg}} \text{ (W/m}^2\text{)} \quad \text{(A4)}$$

This calculation is summarised in Table 4 (row 3).

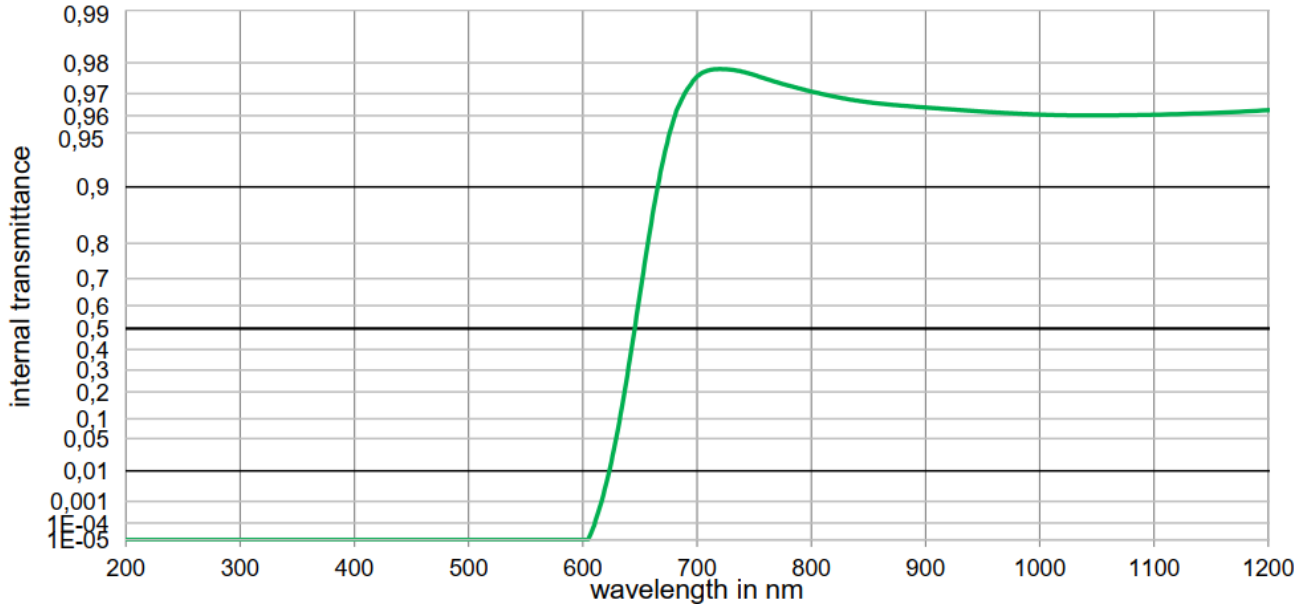

Figure A2. Internal transmittance of red N_2 filter with a 640-650 nm longpass (https://www.schott.com/shop/advanced-optics/en/Matt-Filter-Plates/RG645/c/glass-RG645).